Letter

$CuAg(SO_4)_2$: A doubly strongly correlated altermagnetic three-dimensional analog of the parent compounds of high-T_c cuprates

Harald O. Jeschke,[1] Makoto Shimizu,[2] and Igor I. Mazin[3]

[1]*Research Institute for Interdisciplinary Science, Okayama University, Okayama 700-8530, Japan*

[2]*Department of Physics, Graduate School of Science, Kyoto University, Kyoto 606-8502, Japan*

[3]*Department of Physics and Astronomy, and Quantum Science and Engineering Center, George Mason University, Fairfax, Virginia 22030, USA*

(Received 14 March 2024; revised 1 June 2024; accepted 11 June 2024; published 27 June 2024)

The discovery of high-temperature superconductivity (HTSC) in strongly correlated cuprates opened a new chapter in condensed matter physics, breaking existing stereotypes of what is a material base for a good superconductor ("Matthias rules"), at the same time emphasizing the richness and challenge of strongly correlated physics, personified by the most strongly correlated $3d$ ion, Cu^{2+}. A recently reported new compound, $CuAg(SO_4)_2$, combines in a fascinating way the same ion with the most strongly correlated $4d$ one, Ag^{2+}. In this Letter, we present a detailed analysis of electronic and magnetic properties of this material, and show that it is very different from the HTSC cuprates in several different ways, and opens a door into further research of superconductivity and magnetism, in particular altermagnetism, in strongly correlated materials.

DOI: 10.1103/PhysRevB.109.L220412

Introduction. Four decades ago the world was tantalized by the discovery of high-critical-temperature superconductors. It was soon appreciated that a pivotal role in the physics of these materials was played by the Cu^{2+} ion in a $3d^9$ configuration, a strongly correlated spin-1/2 object with one rather localized hole in the Cu $3d_{x^2-y^2}$ orbital, and that the magnetic interaction between these ions, generated by oxygen-mediated superexchange processes and peaked in two-dimensional (2D) momentum space at $\mathbf{q} = (\pi, \pi)$, is instrumental in understanding its properties [1,2].

The initial microscopic theories of these materials, rather abundant, relied upon a simple single-band Hubbard Hamiltonian, with a Mott insulator as a parent compound [3]. However, it was then realized that, while close to Mott insulators, the parent compounds belonged to a different class, namely charge-transfer insulators (CTIs) [4]. Indeed, the top of the O-p band appeared above the lower Hubbard band (LHB), which led to important ramifications.

The Cu^{2+} valence state occurs in many natural minerals as well as in synthesized compounds. Nevertheless, the peculiar physics associated with the d^9 band occupancy inspired vigorous searches for other d^9 materials. So far, the majority of this activity was associated with Ni^+ compounds, also having a d^9 configuration, albeit less localized than in Cu^{2+} [5,6]. At the same time, solid state chemists had their eyes on a heavier analog of Cu^{2+}, namely Ag^{2+} [7]. The d hole in this state is also highly localized, and materials with Ag^{2+} are truly rare.

Thus, the recent experimental report of a new d^9 compound forming a new, fourth class (counting Cu^{2+}, Ni^+, and Ag^{2+} as the first three), $CuAg(SO_4)_2$ [8], opens an exciting opportunity of a new variation on the old theme: A combination of Cu^{2+} *and* Ag^{2+} in the same compound warrants close attention. Moreover, as we discuss later, magnetic order in this material belongs to a recently discovered class of altermagnets [9,10], adding an additional dimension of interest to this material. It is worth noting that the only altermagnet in this class discussed so far is La_2CuO_4, where altermagnetism appears only because of small rotations of the CuO_6 octahedra [11,12]. In contrast, in $CuAg(SO_4)_2$, as discussed below, altermagnetism appears already in the Cu-Ag sublattice.

One can summarize (Table I) the key differences distinguishing $CuAg(SO_4)_2$ from the parent compounds of cuprate superconductors, as demonstrated and discussed in detail in this Letter.

Given such unique properties of this just recently discovered compound, one should expect more experimental work in the nearest future. The goal of this Letter is to guide and inform this research about fundamental electronic and magnetic properties of this material. In the next section we will present and discuss its electronic structure, then we will turn to magnetic interactions in the system, and demonstrate and explain their highly unusual topology. We will then identify the stable ground state magnetic configuration and discuss its properties, including the character of spin fluctuations once the static order is suppressed (e.g., by doping). Whether such doping will indeed lead to superconductivity is unclear at the moment, but such an opportunity is quite exciting [13].

Crystal structure. The crystal structure is formed by chains aligned along the c axis of octahedral-coordinated Cu and Ag, with edge-sharing octahedra (as opposed to layered perovskite cuprates where octahedra are corner sharing), Fig. 1(a). These chains are bridged by SO_4 radicals, forming "molecular ligands," which are nearly ideal tetrahedra with S nearly central. The intra- as well as interchain hoppings proceed via these tetrahedra. CuO_6 and AgO_6 octahedra are strongly elongated (20% for Cu, 30% for Ag, cf. 28% in La_2CuO_4), so that the d holes reside in a well-defined $d_{x^2-y^2}$ state. Figure 1(b)

 ©2024 American Physical Society

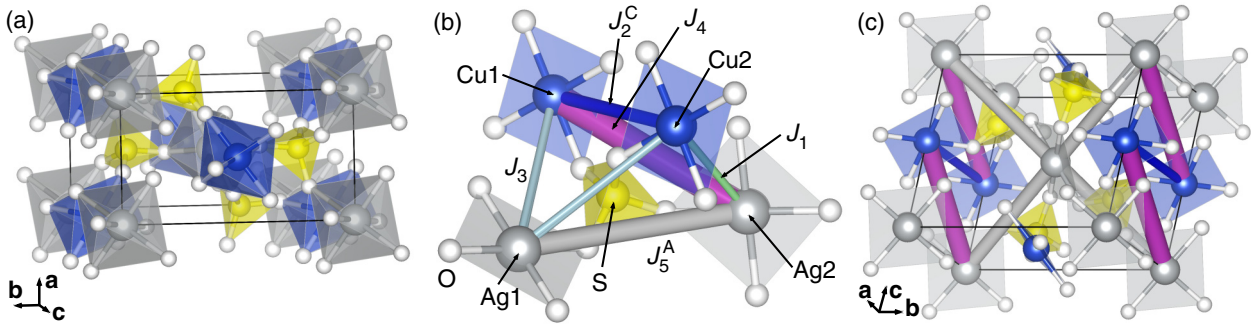

FIG. 1. (a) Crystal structure of $CuAg(SO_4)_2$ (space group $P2_1/n$, No. 14), as reported in Ref. [8]. (b) Structural unit showing only one SO_4 cluster with its nearest neighbor connected via $d_{x^2-y^2}$ orbitals. Cu and Ag sites are only numbered for use in Table II. (c) Illustration of relevant exchange paths in the structure of $CuAg(SO_4)_2$.

shows the minimal connectivity cluster, that is, an individual SO_4 tetrahedron with four metals attached to it. Interestingly, all four metal ions are positioned geometrically different, as Table II illustrates, and form different bond angles.

Electronic structure. We perform all electronic structure calculations using the full potential local orbital (FPLO) basis set [14] in combination with a generalized gradient approximation (GGA) exchange correlation functional [15]. We use a number of k points that ensures full convergence of the respective quantities which is $12 \times 12 \times 12$ for electronic structures and Fermi surfaces and $4 \times 4 \times 4$ for the large supercells used in energy mapping. The calculated band structure is shown in Fig. 2, and the corresponding density of states (DOS) in Fig. 3. For comparison, the DOS for La_2CuO_4 (calculated with the same setup) is shown in the Supplemental Material [16]. Several interesting features manifest themselves. First, due to much longer hopping paths, and strong covalent bonding in the SO_4 cluster, O bands are pushed up, compared to HTSC cuprates, and are twice narrower. As a result, 12 O p bands are separated from the rest by a full gap, and are much more pure O p than in the cuprates, while the charge-transfer (CT) gap is much larger (1.3 eV vs 0.4 eV, for the same parameter choice) and the upper Hubbard bands much narrower in $CuAg(SO_4)_2$. As a result, the metal states are more correlated, and the CT character more pronounced than in the cuprates, promising interesting ramifications.

These new features can also be traced down to the fact that the actual "ligand" in this system is in fact the sulfate ion, which has an interesting molecular orbital structure [17,18]: one triple-degenerate t_1 orbital in each spin, which is pure O $2p$ by symmetry, and also a mixed O-S one, also a triplet, $3t_2$. The latter is the higher occupied orbital *if S 3d is not included* [17]. However, the high-lying S $3d$ pushes this state down [17], resulting in a clear separation of the upper half of the O bands, well above the metal d bands, and the lower half, overlapping the latter. What is important here is that if the system is doped by holes, they will be purely O $2p$, as opposed to cuprates, where they are considerably mixed with Cu $3d$.

One other observation from Fig. 2 is that the d bands along the Γ-R line are spin split, despite the material being antiferromagnetic (AFM), and centrosymmetric (for further evidence, see Fig. S3 in Supplemental Material [16]). Indeed, one can observe that the symmetry operation that maps the spin-up and spin-down sublattices in the $P2_1/n$ group is the n glide $(x, y, z) \rightarrow (x + \frac{1}{2}, -y + \frac{1}{2}, z + \frac{1}{2})$, while inversion maps each spin upon itself. Thus, the "glide + space inversion + time reversal" operations do not change the

TABLE I. Comparison between parent materials of cuprate superconductors and $CuAg(SO_4)_2$.

	Parent cuprates	$CuAg(SO_4)_2$
Strongly correlated species	One (Cu)	Two (Cu, Ag)
Excitation gap	Intermediate, closer to CT	Strongly CT
Leading superexchange path	Cu-O-Cu	M-SO_4-M
Leading superexchange neighbors	First	3rd, 5th, and 6th
Leading superexchange length[a]	~2.7–2.8 Å	5.7, 6.0, 4.7 Å
Dimensionality	2D	3D
Leading spin fluctuations	$\mathbf{q} = (\pi, \pi)$	$\mathbf{q} = (0, 0, 2\pi)$[b]
Altermagnetism	Sometimes[c]	Yes[d]

[a]In order of decreasing strength.
[b]In the extended Brillouin zone, corresponding to the intracell magnetic order.
[c]In La_2CuO_4 and similar materials, due to O octahedra rotations.
[d]Regardless of the presence of ligands.

TABLE II. Top: Angles formed by the M-O-S in degrees. Bottom: Angles θ in degrees, distance d in Å of the corresponding path, and calculated (see the section of magnetic interactions for details) exchange coupling constants J in K formed by M-S-M.

M	M-O-S		
Cu1	135		
Cu2	137		
Ag1	123		
Ag2	140		
	θ (deg)	d (Å)	J (K)
Cu1-S-Cu2	96	4.73	34
Cu1-S-Ag1	102	4.96	5
Cu1-S-Ag2	122	5.73	168
Cu2-S-Ag1	102	4.96	5
Cu2-S-Ag2	66	3.58	−3
Ag1-S-Ag2	134	6.02	92

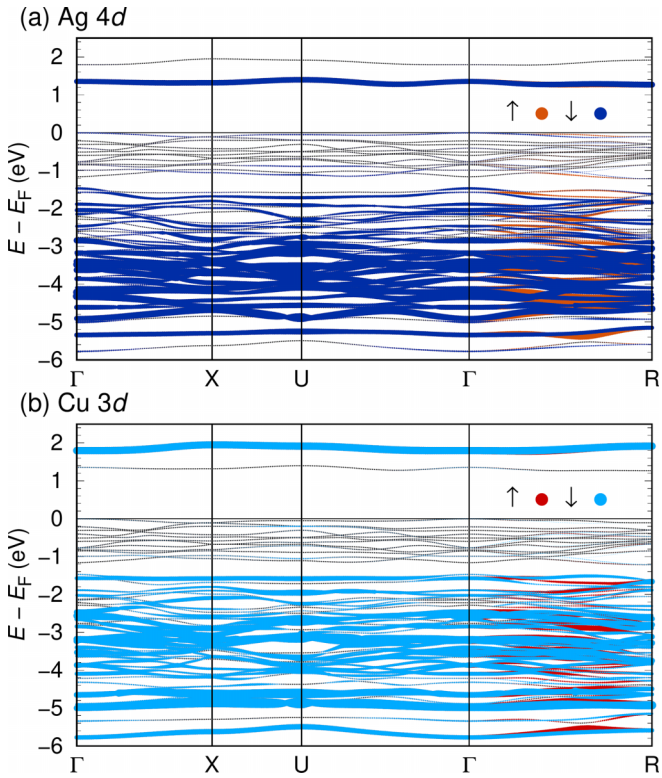

FIG. 2. GGA + U band structure of CuAg(SO$_4$)$_2$ in the lowest-energy AFM state. Colors red (spin ↑) and blue (spin ↓) indicate (a) Ag 4d orbital weights and (b) Cu 3d orbital weights. The altermagnetic property of CuAg(SO$_4$)$_2$ is clear from the spin splitting along the Γ-R path. High symmetry points are $X = (1/2, 0, 0)$, $U = (1/2, 0, 1/2)$, $R = (1/2, 1/2, 1/2)$.

magnetic structure. This operation will change the electronic state at (k_x, k_y, k_z) as $(k_x, k_y, k_z, \uparrow) \rightarrow (k_x, -k_y, k_z, \uparrow) \rightarrow (-k_x, k_y, -k_z, \uparrow) \rightarrow (k_x, -k_y, k_z, \downarrow)$ [19]. Thus, the Kramers degeneracy is preserved if $k_y = 0$ or π, consistent with the

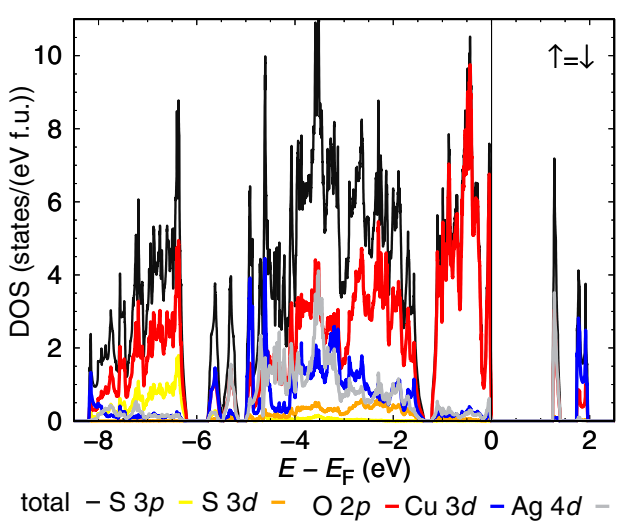

FIG. 3. GGA + U density of states per spin of CuAg(SO$_4$)$_2$ in the lowest-energy AFM state. Spin ↑ and spin ↓ are identical so only spin ↑ is shown.

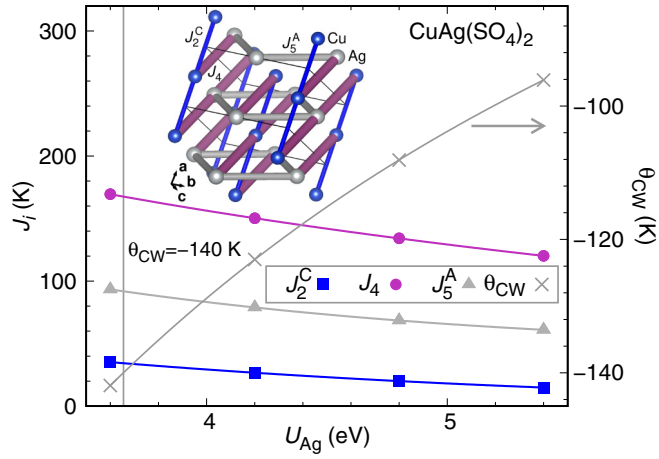

FIG. 4. DFT energy mapping result for CuAg(SO$_4$)$_2$. Most important exchange interactions for four different values of on-site interaction U_{Ag} at fixed Hund's rule coupling strengths $J_{\mathrm{H}} = 1$ eV for Cu and $J_{\mathrm{H}} = 0.75$ eV for Ag. U_{Ag} is fixed at 75% of U_{Cu}. Inset: Exchange paths of CuAg(SO$_4$)$_2$ as defined by the three dominant exchange interactions. The width of the bonds is chosen so that cross section is proportional to the strength of the coupling.

fact that the spin splitting does not occur along the Γ-X-U-Γ line in Fig. 2 and that they are spin split along Γ-R. This is the condition for altermagnetism, a new phenomenon actively discussed recently [10,20–24]. It is worth noting that some of the cuprates, most notably La$_2$CuO$_4$, are also altermagnets, but there this feature appears as a result of the CuO$_6$ octahedra rotations [11,12], and disappears when the structure becomes tetragonal under doping. Here, however, it is robust and present even if ligands are entirely removed (the Cu-Ag sublattice still has the same symmetry).

Magnetic interactions. We determine parameters of the Heisenberg Hamiltonian $H = \sum_{i<j} J_{ij} \mathbf{S}_i \cdot \mathbf{S}_j$ for CuAg(SO$_4$)$_2$ using density functional theory (DFT) energy mapping. This approach has provided very good results for many Cu^{2+} $S = 1/2$ magnets [25–27], so we can expect it to work for CuAg(SO$_4$)$_2$ as well. It is based on a DFT + U correction [28] in order to account for strong correlations on Cu 3d and Ag 4d orbitals. We make sure to capture all relevant exchange interactions by resolving all couplings up to twice the nearest-neighbor Cu-Ag distance. For this purpose, we use a fivefold supercell containing ten formula units. For the DFT + U functional, we need on-site interactions and values of the Hund's rule coupling for both Cu^{2+} and Ag^{2+}. Between Cu 3d orbitals and Ag 4d orbitals, we introduce a factor 0.75 which is reasonable to account for the better screening in the heavier ion. For Cu^{2+}, we use the typical value $J_{\mathrm{H}}^{\mathrm{Cu}} = 1$ eV that has yielded good agreement with experiment in many cases. Figure 4(a) shows the result of the energy mapping for four values of U.

Other exchange interactions besides the three we show are 3% of the dominant coupling J_4 or less (Table III). We select values of $U_{\mathrm{Ag}} = 3.65$ eV, $U_{\mathrm{Cu}} = 4.87$ eV by demanding that the the full set of couplings matches the experimentally determined Curie-Weiss temperature of CuAg(SO$_4$)$_2$ which is $\theta_{\mathrm{CW}} = -140$ K [8]. Note that these U values should be

TABLE III. Exchange parameters for $CuAg(SO_4)_2$ determined by DFT-based energy mapping. The on-site interaction values $U_{Ag} = 3.65$ eV and $U_{Cu} = 4.87$ eV are chosen in order to match the experimental value of the Curie-Weiss temperature of $\theta_{CW} = -140$ K [8]. The U_{Cu} is smaller than typical values for Cu^{2+} which are often in the range 6 eV $\leqslant U \leqslant$ 8 eV; this occasionally happens when U is chosen to match a θ_{CW} energy scale in energy mapping.

Name	J_1	J_2^A	J_2^C	J_3	J_4	J_5^A	J_5^C	J_6	J_7^A	J_7^C	J_8^A	J_8^C	J_{10}	J_{13}	J_{16}^A	J_{16}^C
$M1\,M2$	AgCu	AgAg	CuCu	AgCu	AgCu	AgAg	CuCu	AgCu	AgAg	CuCu	AgAg	CuCu	AgCu	AgCu	AgAg	CuCu
$d_{M1\,M2}$ (Å)	3.579	4.734		4.961	5.727	6.017		6.134	6.215		7.158		8.332	8.846	9.266	
J (K)	−3	3	34	5	168	92	−1	−3	0	−4	−2	0	0	0	1	0

viewed as internal local density approximation (LDA) $+U$ parameters and not as spectroscopic U values; they would be chosen differently if future experiments lead to a revision of the θ_{CW} value. The inset of Fig. 4 illustrates the lattice defined by J_4, $J_5^A = 0.55J_4$ and $J_2^C = 0.20J_4$. The Hamiltonian is dominated by antiferromagnetic Cu-Ag chains (purple) which are linked by AFM Ag-Ag square lattices. These two couplings can be satisfied by an AFM state where both Cu and Ag sublattices are AFM. However, the third strongest (but considerably smaller) coupling, an AFM Cu-Cu exchange, is moderately frustrating this Hamiltonian. We can compare our Hamiltonian parameters to the result obtained by Domanski *et al.* [8] $J_4 = 120$ K, $J_5^A = 1.08J_4$, $J_2^C = -0.06J_4$. A likely reason for the difference is that the approach of Ref. [8] of solving eight equations for seven exchange interactions can go astray with small inaccuracies of any one of the calculated energies.

This result seems, on the first glance, counterintuitive. The strongest coupling comes from the fifth neighbors, and the two shortest bonds contribute practically nothing. To understand this we recall that the active orbitals here are $x^2 - y^2$, and replot Fig. 1(a) using instead of the metal-centered octahedra only the squares corresponding to these orbitals [Fig. 1(b)]. One can see that these orbitals do not overlap on any oxygen, thus not generating any M-O-M superexchange, but only via SO_4^{2-} ions. This yields five longer-range superexchange paths, which include the three leading ones, plus two more that appear to be numerically small due to accidental cancellation of various hopping processes. As discussed in the previous section, electronically this material is in a strong charge-transfer regime, so that instead of the standard Anderson's superexchange proportional to $t^4/(E_d - E_p)^2U$, where $E_d - E_p \gg U$, and t is the characteristic metal-ligand hopping, one gets [29] t^4/Δ^3, with $\Delta \ll U$ (note that the charge-transfer energy Δ is smaller because the highest occupied level in sulfate is higher than in oxygen). Therefore, despite a relatively small effective M-S hopping the resulting interaction is sizable.

Susceptibility. We analyze the Hamiltonian by defining a strong coupling susceptibility [30] as $\chi(\mathbf{q}, T) = 1/[T + J(\mathbf{q})]$, where

$$\begin{aligned} J(\mathbf{q}) = {} & 2J_1 \cos\frac{q_z}{2} + \left(J_2^A + J_2^C\right)\cos q_x \\ & + \left(2J_3 \cos\frac{q_x}{2} + \left(J_7^A + J_7^C\right)\cos\frac{q_x - q_z}{2}\right. \\ & \left. + \left(J_5^A + J_5^C\right)\cos\frac{q_x + q_z}{2}\right) 2\cos\frac{q_y}{2} \\ & + 2J_4 \cos\left(q_x + \frac{q_z}{2}\right) + 2J_6 \cos\left(q_x - \frac{q_z}{2}\right) \\ & + \left(J_8^A + J_8^C\right)\cos q_z. \end{aligned}$$

This susceptibility has maxima that are extended diagonally around $\mathbf{q} = (0, 0, 2\pi)$ in the $(q_x, 0, q_z)$ plane as shown in Fig. 5(a). There are weak maxima, marked by red dots, which are shifted from $\mathbf{q} = (0, 0, 2\pi)$ to $\mathbf{q} = (0.603, 0, 0.986)\pi$ and $\mathbf{q} = (-0.603, 0, 3.014)\pi$.

Classical Monte Carlo. We perform classical Monte Carlo calculations for the Heisenberg Hamiltonian parameters given in Table III. We perform the standard single spin-flip technique with the Metropolis updates. The result is shown

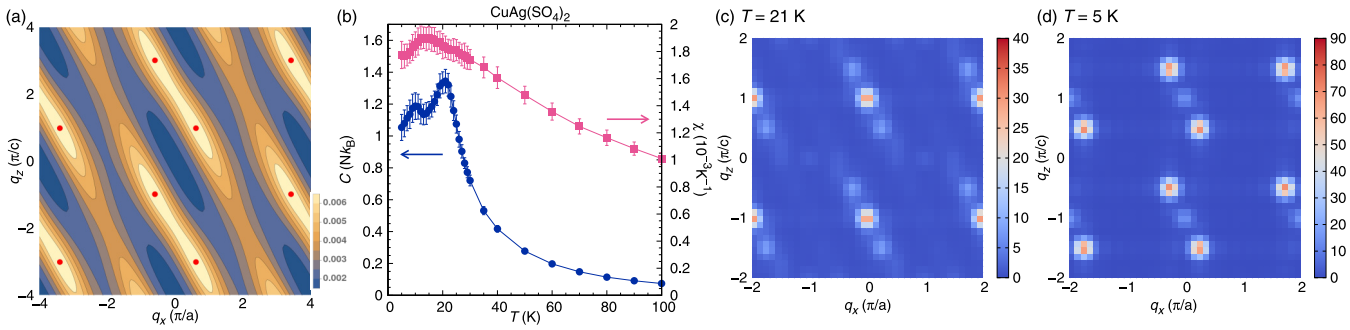

FIG. 5. Susceptibility and classical Monte Carlo (CMC) results for $CuAg(SO_4)_2$. (a) Susceptibility $\chi(\mathbf{q}, T)$ of $CuAg(SO_4)_2$ at $T = 300$ K estimated using Eq. (1). (b) CMC specific heat and susceptibility. (c) and (d) correspond to spin structure factors at $T = 21$ K and $T = 5$ K, respectively. Note that for the $\mathbf{q}$ vectors in (a), (c), and (d) we neglect the small monoclinic angle of 94° and the difference in a and c lattice parameters.

in Figs. 5(b)–5(d). The specific heat shows two peaks at $T = 21$ K and at $T = 10$ K. This indicates that even though the two dominant exchange couplings J_4 and J_5^{A} are unfrustrated, the frustrating coupling J_2^{C} leads to a significant reduction of the ordering temperature compared to the Curie-Weiss temperature of $\theta_{\mathrm{CW}} = -140$ K. This is in good agreement with experiment where the material shows a pronounced ordering peak at $T = 40.4$ K. The peaks in the susceptibility [Fig. 5(b)] are less clearly separated. The type of ordering can be understood from Figs. 5(c) and 5(d). Upon lowering the temperature, the dominant instability is at $\mathbf{q} = (0, 0, 2\pi)$ [Fig. 5(c)]. When T is lowered further, the weak corrections due to the frustration present in the Hamiltonian kick in, increasing the weight slightly away from $\mathbf{q} = (0, 0, 2\pi)$ [Fig. 5(d)]. Thus, the second ordering peak corresponds to the weak maxima marked by red dots in Fig. 5(a).

Conclusions. We have investigated the electronic structure and magnetic properties of the recently discovered $CuAg(SO_4)_2$ compound, which combines strongly correlated Cu^{2+} and Ag^{2+} ions. This material bears many similarities with high-T_c cuprates, but also a number of remarkable differences, outlined in Table I. The differences stem from the fact that in this compound the sulfate ion SO_4^{2-} plays the ligand role, as opposed to oxygen. As a result, the relevant hopping and exchange paths are longer range, the antiferromagnetic ground state is highly unusual, and potential hole doping proceeds via pure O p bands (rather than a hybridized Cu-O band, as in the cuprates). In addition, the ground state is altermagnetic, that is to say, sports spin-split Cu d bands (which, however, as mentioned, are considerably removed from the Fermi level).

This collection of highly unusual properties make $CuAg(SO_4)_2$ a fertile playground for exotic magnetism and superconductivity (under doping); while these are beyond the scope of the current Letter, we hope that it will inspire further experimental and theoretical studies in this direction.

Acknowledgments. I.M. was supported by the Army Research Office under Cooperative Agreement No. W911NF-22-2-0173. M.S. was supported by Graduate School of Science, Kyoto University under Ginpu Fund and by JSPS KAKENHI Grants No. 22H01181 and No. 23K19032. Part of the computation in this work has been done using the facilities of the Supercomputer Center, the Institute for Solid State Physics, the University of Tokyo. We acknowledge fruitful discussions with L. Jaubert and C.-g. Oh. We also thank G. Khalliulin for a critical reading of the manuscript. Some of the images in this Letter were created using VESTA software [31].

[1] E. Dagotto, Correlated electrons in high-temperature superconductors, Rev. Mod. Phys. **66**, 763 (1994).
[2] M. Imada, A. Fujimori, and Y. Tokura, Metal-insulator transitions, Rev. Mod. Phys. **70**, 1039 (1998).
[3] P. A. Lee, N. Nagaosa, and X.-G. Wen, Doping a Mott insulator: Physics of high-temperature superconductivity, Rev. Mod. Phys. **78**, 17 (2006).
[4] J. Zaanen, G. A. Sawatzky, and J. W. Allen, Band gaps and electronic structure of transition-metal compounds, Phys. Rev. Lett. **55**, 418 (1985).
[5] P. Hansmann, X. Yang, A. Toschi, G. Khaliullin, O. K. Andersen, and K. Held, Turning a nickelate Fermi surface into a cupratelike one through heterostructuring, Phys. Rev. Lett. **103**, 016401 (2009).
[6] D. Li, K. Lee, B. Y. Wang, M. Osada, S. Crossley, H. R. Lee, Y. Cui, Y. Hikita, and H. Y. Hwang, Superconductivity in an infinite-layer nickelate, Nature (London) **572**, 624 (2019).
[7] J. Gawraczyński, D. Kurzydlowski, R. A. Ewings, S. Bandaru, W. Gadomski, Z. Mazej, G. Ruani, I. Bergenti, T. Jaroń, A. Ozarowski, S. Hill, P. J. Leszczyński, K. Tokár, M. Derzsi, P. Barone, K. Wohlfeld, J. Lorenzana, and W. Grochala, Silver route to cuprate analogs, Proc. Natl. Acad. Sci. USA **116**, 1495 (2019).
[8] M. Domański, Z. Mazej, and W. Grochala, A unique two-dimensional silver(II) antiferromagnet $Cu[Ag(SO_4)_2]$ and perspectives for its further modifications, Chem. Eur. J. **29**, e202302042 (2023).
[9] I. Mazin (The PRX Editors), Editorial: Altermagnetism—a new punch line of fundamental magnetism, Phys. Rev. X **12**, 040002 (2022).
[10] L. Šmejkal, J. Sinova, and T. Jungwirth, Emerging research landscape of altermagnetism, Phys. Rev. X **12**, 040501 (2022).
[11] M. Naka, Y. Motome, and H. Seo, Perovskite as a spin current generator, Phys. Rev. B **103**, 125114 (2021).
[12] L. Šmejkal, J. Sinova, and T. Jungwirth, Beyond conventional ferromagnetism and antiferromagnetism: A phase with nonrelativistic spin and crystal rotation symmetry, Phys. Rev. X **12**, 031042 (2022).
[13] I. I. Mazin, Notes on altermagnetism and superconductivity, arXiv:2203.05000.
[14] K. Koepernik and H. Eschrig, Full-potential nonorthogonal local-orbital minimum-basis band-structure scheme, Phys. Rev. B **59**, 1743 (1999).
[15] J. P. Perdew, K. Burke, and M. Ernzerhof, Generalized gradient approximation made simple, Phys. Rev. Lett. **77**, 3865 (1996).
[16] See Supplemental Material at http://link.aps.org/supplemental/10.1103/PhysRevB.109.L220412 for additional DFT results, more analysis of the altermagnetism, and details on the classical Monte Carlo calculations, which includes Refs. [8,19,32–37].
[17] D. M. Bishop, Molecular orbital energy levels for the sulfate ion, Theor. Chim. Acta **8**, 285 (1967).
[18] G. Höjer, S. Meza-Höjer, and G. Hernández de Pedrero, A CNDO study of the electronic structure of oxyanions XO_4^{n-} with X = Si, P, S, Cl, Ge, As, Se and Br, Chem. Phys. Lett. **37**, 301 (1976).
[19] H. Kim, K. Shiozaki, and S. Murakami, Glide-symmetric magnetic topological crystalline insulators with inversion symmetry, Phys. Rev. B **100**, 165202 (2019).
[20] M. Naka, S. Hayami, H. Kusunose, Y. Yanagi, Y. Motome, and H. Seo, Spin current generation in organic antiferromagnets, Nat. Commun. **10**, 4305 (2019).
[21] K.-H. Ahn, A. Hariki, K.-W. Lee, and J. Kuneš, Antiferromagnetism in RuO_2 as d-wave Pomeranchuk instability, Phys. Rev. B **99**, 184432 (2019).

[22] S. Hayami, Y. Yanagi, and H. Kusunose, Momentum-dependent spin splitting by collinear antiferromagnetic ordering, J. Phys. Soc. Jpn. **88**, 123702 (2019).

[23] L. Šmejkal, R. González-Hernández, T. Jungwirth, and J. Sinova, Crystal time-reversal symmetry breaking and spontaneous Hall effect in collinear antiferromagnets, Sci. Adv. **6**, eaaz8809 (2020).

[24] S. Hayami, Y. Yanagi, and H. Kusunose, Bottom-up design of spin-split and reshaped electronic band structures in antiferromagnets without spin-orbit coupling: Procedure on the basis of augmented multipoles, Phys. Rev. B **102**, 144441 (2020).

[25] S. Chillal, Y. Iqbal, H. O. Jeschke, J. A. Rodriguez-Rivera, R. Bewley, P. Manuel, D. Khalyavin, P. Steffens, R. Thomale, A. T. M. N. Islam, J. Reuther, and B. Lake, Evidence for a three-dimensional quantum spin liquid in $PbCuTe_2O_6$, Nat. Commun. **11**, 2348 (2020).

[26] L. Heinze, H. O. Jeschke, I. I. Mazin, A. Metavitsiadis, M. Reehuis, R. Feyerherm, J.-U. Hoffmann, M. Bartkowiak, O. Prokhnenko, A. U. B. Wolter, X. Ding, V. S. Zapf, C. Corvalán Moya, F. Weickert, M. Jaime, K. C. Rule, D. Menzel, R. Valentí, W. Brenig, and S. Süllow, Magnetization process of atacamite: A case of weakly coupled $S = 1/2$ sawtooth chains, Phys. Rev. Lett. **126**, 207201 (2021).

[27] M. Hering, F. Ferrari, A. Razpopov, I. I. Mazin, R. Valentí, H. O. Jeschke, and J. Reuther, Phase diagram of a distorted kagome antiferromagnet and application to Y-kapellasite, npj Comput. Mater. **8**, 10 (2022).

[28] A. I. Liechtenstein, V. I. Anisimov, and J. Zaanen, Density-functional theory and strong interactions: Orbital ordering in Mott-Hubbard insulators, Phys. Rev. B **52**, R5467 (1995).

[29] G. Khaliullin, Orbital order and fluctuations in Mott insulators, Prog. Theor. Phys. Suppl. **160**, 155 (2005).

[30] J. Otsuki, K. Yoshimi, H. Shinaoka, and Y. Nomura, Strong-coupling formula for momentum-dependent susceptibilities in dynamical mean-field theory, Phys. Rev. B **99**, 165134 (2019).

[31] K. Momma and F. Izumi, *VESTA3* for three-dimensional visualization of crystal, volumetric and morphology data, J. Appl. Crystallog. **44**, 1272 (2011).

[32] H. O. Jeschke, F. Salvat-Pujol, E. Gati, N. H. Hoang, B. Wolf, M. Lang, J. A. Schlueter, and R. Valentí, Barlowite as a canted antiferromagnet: Theory and experiment, Phys. Rev. B **92**, 094417 (2015).

[33] K. Iida, H. K. Yoshida, A. Nakao, H. O. Jeschke, Y. Iqbal, K. Nakajima, S. Ohira-Kawamura, K. Munakata, Y. Inamura, N. Murai, M. Ishikado, R. Kumai, T. Okada, M. Oda, K. Kakurai, and M. Matsuda, $q = 0$ long-range magnetic order in centennialite $CaCu_3(OD)_6Cl_2 \cdot 0.6D_2O$: A spin-$\frac{1}{2}$ perfect kagome antiferromagnet with J_1-J_2-J_d, Phys. Rev. B **101**, 220408(R) (2020).

[34] G. Kresse and J. Hafner, *Ab initio* molecular dynamics for liquid metals, Phys. Rev. B **47**, 558 (1993).

[35] G. Kresse and J. Furthmüller, Efficiency of *ab-initio* total energy calculations for metals and semiconductors using a plane-wave basis set, Comput. Mater. Sci. **6**, 15 (1996).

[36] G. Kresse and J. Furthmüller, Efficient iterative schemes for *ab initio* total-energy calculations using a plane-wave basis set, Phys. Rev. B **54**, 11169 (1996).

[37] G. Kresse and D. Joubert, From ultrasoft pseudopotentials to the projector augmented-wave method, Phys. Rev. B **59**, 1758 (1999).